DOI 10.31489/2023No1/12-19
UDC 538.9

STUDY OF THE INITIAL MAGNETIC PERMEABILITY OF LiTiZnMn FERRITES OBTAINED BY LIQUID-PHASE SINTERING UNDER RADIATION-THERMAL AND THERMAL CONDITIONS

Surzhikov A.P., Lysenko E.N., Malyshev A.V.

Tomsk Polytechnic University, Tomsk, Russia, malyshev@tpu.ru

The measuring the temperature dependence of the initial permeability was used to study the features of phase and structural transformations in lithium-titanium ferrites as a function of time, heating and cooling rates, and the temperature of liquid-phase sintering under thermal and radiation-thermal heating. Ferrite was synthesized from powder mixture by solid-phase synthesis. A low-melting additive bismuth dioxide was used to obtain the ferrite ceramics by liquid-phase sintering. RT sintering was carried out by heating the samples with a pulsed (1.5–2.0) MeV electron beam. It was established that the additive leads to a less defective state of sintered ferrites, while the action of radiation enhances this effect in the early stages of sintering. The regularities of the influence of the heating and cooling rates of compacted samples on the change in the initial magnetic permeability of sintered ferrites are established.

Keywords: lithium ferrite, liquid-phase sintering, electron beam, high temperature, heating and cooling rates, initial magnetic permeability.

Introduction

The fundamental requirements for ferrite materials production are their good electromagnetic characteristics, which depend on the chemical composition of the reagents and ferrite technology. The main operation of the ferrites production by ceramics technology is the extremely long sintering of compacted samples molded from synthesized powders.

The operations used to activate the sintering of ferrites, including the two-stage introduction of various components, the addition of ferrite powders of the same composition to the samples, the presence of a liquid phase, forced sintering, the application of ultrasound to the sintering process [1–4], are accompanied by an increased probability of impurity phases entering the product composition, worsening the chemical and structural homogeneity of the material and, accordingly, the electromagnetic properties. At the same time, it is not always possible to reduce the content of impurity phases by selecting the sintering temperature regime, especially in the case of thermally unstable compounds, such as lithium ferrispinels.

In recent years, the impact of ionizing radiation fluxes has been developed in the production and modification of materials. In this case, the fundamental phenomenon of a multiple increase in the process of synthesis of multicomponent powder materials [5–13] and sintering [14–24] under radiation-thermal (RT) conditions was discovered. The processes of lithium-titanium ferrites sintering have been most fully studied under such specific conditions of the combined action of high temperatures and intense electron flows [25–29]. Here, the regularities in compaction of ferrites have been established and a multiple increase in the rate of lithium-titanium ferrites sintering has been shown in [30, 31].

The ultimate goal of any technology for the ferrites production is to achieve a given level of operational properties, including the main functional magnetic characteristics. Therefore, the influence of various factors on the formation of the ferrites magnetic characteristics under RT sintering is of particular interest.

From this point of view, data on phase transformations in ferrites during RT sintering are important. In the case of obtaining lithium ferrites, the complexity of the X-ray phase analysis is due to the overlap of the main reflections from the $LiFe_5O_8$, $LiFeO_2$, Fe_3O_4 phases, which can form during synthesis or sintering. Therefore, the method of measuring the temperature dependence of the initial permeability is promising for studying the features of phase transformations in lithium ferrite ceramics.

For this purpose, in [32], the radiation contribution to the ferrite electromagnetic parameters formation was established from a comparison of the temperature dependences of the initial permeability (μ_i) of lithium

ferrites obtained by RT and thermal (T) solid-phase sintering. Since the technology of liquid-phase sintering is widely used in ferrites production, the next stage of our work is to study the same patterns in the presence of a liquid-phase component in ferrites under the same RT and T conditions. In addition, in order to establish the effects of low-melting additive, the obtained data on liquid-phase sintering of lithium ferrites were compared with the data obtained during solid-phase sintering. Since, before the pressing stage, a solution of polyvinyl alcohol (PVA) and a low-melting additive of bismuth oxide (Bi_2O_3) were introduced into the composition of ferrite powders, the influence of cooling and heating modes of ferrites during sintering on the temperature dependence of μ_i of samples was studied.

1. Experimental part

1.1 Materials

In this work, experimental samples of lithium-titanium ferrite were prepared according to the following proven technological stages. Ferrites are synthesized from a mechanical mixture of oxides and carbonates containing (in wt %): Fe_2O_3 – 59.8; Li_2CO_3 – 11.2; TiO_2 – 18.7; ZnO – 7.6; $MnCO_3$ – 2.7. After weighing the above components, they were ground together and wet mixed by a vibrating mill for 1 hour using distilled water, which was added to the powder in a weight ratio of 1:2. The milled mixture was dried at 80 °C for 24 h and then passed through a 0.7 sieve. The distilled water was introduced into the resulting powder in an amount of 10 wt% of the powder, and it was briquetted. The briquettes were heated in thermal furnaces at a rate of 200 °C/h to 900 °C, kept at this temperature for 6 hours, and cooled to room temperature. After that, they were crushed, sieved through a 0.9 sieve and mixed by a vibrating mill for 45 min. A low-melting additive in the form of a suspension based on Bi_2O_3 (0.22 wt %) dissolved in concentrated nitric acid was added to the powder and homogenized by milling in a ball mill for 4 h. Then, a 10% solution of polyvinyl alcohol (PVA) was added to the synthesized ferrite in an amount of 12 wt. % of the ferrite powder, and the thus prepared powder was alternately rubbed through 0.7 and 0.45 sieves. Press samples were made by cold one-sided pressing in the toroidal form with an outer diameter of 18 mm, an inner diameter of 14 mm, and a height of 2 mm. The pressing pressure is selected, as a rule, experimentally for each specific ferrite composition according to the established dependence of the bulk density ρ of the samples on the pressing pressure. In this work, a pressing pressure of 130 MPa and a holding time of the samples under this pressure of 1 min were used.

1.2 Characterization techniques

RT-sintering was carried out by heating the samples with a pulsed (1.5–2.0) MeV electron beam using an ILU-6 accelerator. The beam current in the pulse was (0.5–0.9) A, the duration of the irradiation pulse was 500 μs, the pulse repetition rate was (5–50) Hz, and the heating rate of the samples was 1000 °C/min. The samples were placed in a cell, which was a box made of lightweight chamotte with a bottom wall thickness of 15 mm. From the side of the electron beam, the cell was covered with a radiation-transparent protector with a mass thickness of 0.1 g/cm. The temperature was measured using a thermocouple located in a control sample that was placed in close proximity to the sintered ferrite samples.

Thermal sintering of the samples was carried out using a chamber electric furnace. For this, the samples were placed in a preheated furnace, which ensured a heating rate comparable to that of an electron beam. The cell design and temperature control technique are similar to those used in RT sintering. Both modes of sintering were carried out in air. Based on the analysis of literature data on methods for measuring the initial magnetic permeability (μ_i), a method based on measuring the inductance of ring cores in an alternating magnetic field was used [33]. On samples sintered in different modes, a single-layer winding was evenly distributed around the perimeter of the core. The measurement of μ_i was carried out using a standard inductance meter at a frequency of 1 MHz when the sample cooled down from a temperature obviously higher than the Curie temperature (about 350 °C). From the temperature dependence of the inductance, the temperature dependence of μ_i was determined by the equation [32, 33].

2. Results and discussion

Figure 1 shows the temperature dependences of μ_i for the samples sintered at 1373 K under thermal and radiation-thermal conditions. Qualitatively, these dependences are identical to similar ones for solid-phase sintered (that is, without Bi_2O_3) samples presented in [32], since they are based on the same magnetization

.

processes. It can be seen from Fig. 1 that the values of μ_i at the maxima of the curves exceed the corresponding values of μ_i in the samples sintered without the addition of Bi_2O_3. This is especially evident during sintering in the T mode, as well as in the early stages of sintering in the RT mode.

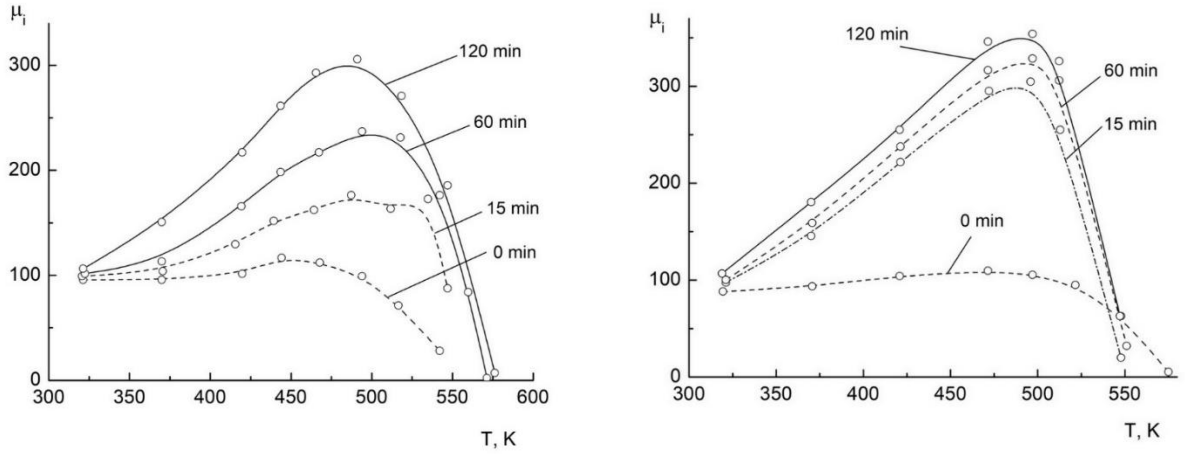

a) b)

Fig.1. Temperature dependence of initial permeability of the ferrite samples sintered at 1373 K for different times by T (a) and RT (b) method

The dependences of the maximum value (from the temperature dependence) of the initial permeability, $\mu_{i\,max}$, of ferrite on the duration of sintering are shown in Figure 2. When sintering in the RT mode, the rate of increase in $\mu_{i\,max}$ at the beginning of sintering significantly exceeds the growth rate $\mu_{i\,max}$ for samples sintered in the T mode. When the sintering time is more than 20 min, the growth rates $\mu_{i\,max}$ are equalized for both types of sintering. Since the value of $\mu_{i\,max}$ is inversely proportional to the integral defectiveness of ferrite samples, it can be concluded that the sintering of samples with the addition of Bi_2O_3 leads to a more defect-free state in ferrite. In this case, the action of radiation at RT heating enhances this effect in the early stages of sintering.

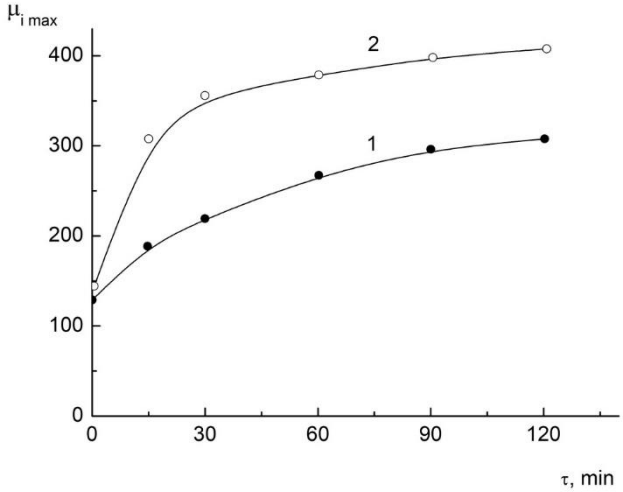

Fig.2. Dependence of the maximum value of the initial permeability of ferrite (from the temperature dependence) on the duration of sintering at 1373 K via T (curve 1) и RT (curve 2) modes

Considering that the early stages of liquid-phase sintering are caused by such processes as the dissolution of a solid in the contact zone, the dissolution of protrusions and irregularities of particles, and the rearrangement of particles [34], it should be assumed that under radiation heating, these processes are intensified. This conclusion is consistent with the results obtained from the study of the kinetics of liquid-phase compaction of powder materials under the action of an electron beam and presented in [35].

Figure 3 shows the differential temperature dependences of μ_i near the Curie temperature for samples containing Bi_2O_3. These samples contain two magnetic phases, which correspond to the maxima of the decay

rate $d\mu_i/dT$ at temperatures of 537 K and 548 K. In the early stages of sintering (up to 15 min), the low-temperature magnetic phase dominates in the T mode, and the high-temperature one dominates in the RT mode. At a sintering time of $\tau = 30$ min, the phase ratio is equalized for both sintering modes, and at $\tau \geq 60$ min, the high-temperature phase predominates regardless of the mode.

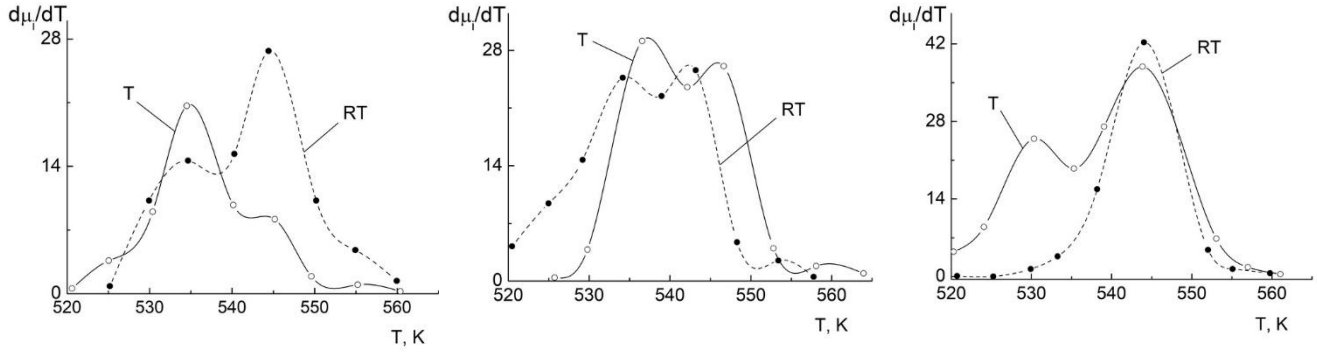

a) b) c)

Fig.3. Differential temperature dependence of the initial permeability near the Curie temperature for samples sintered at 1373 K for 15 (a), 30 (b) and 60 (c) min via T and RT modes

From these results, the peculiarity of homogenization of LiTiZnMn ferrite in the presence of Bi_2O_3 is concluded: the rate of chemical homogenization is higher compared to RT homogenization, and at $\tau > 60$ min, the phase compositions are equalized. At the nonisothermal stage of sintering and in the isothermal mode up to $\tau \sim 15$ min, the rate of RT homogenization remains high. To increase the sintering rate and intensify phase transformations in ceramic technology, elevated firing temperatures are used. But, as noted above, this method is not suitable for lithium ferrites because of their low thermal stability. In order to verify this position, the temperature dependences of μ_i and $d\mu_i/dT$ were measured for the samples sintered at a temperature of 1473 K. Figure 4 and Figure 5 show these dependencies.

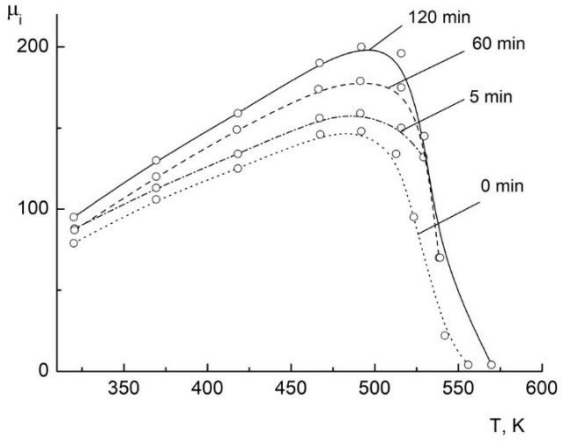

Fig.4. Temperature dependence of the initial permeability of the ferrite sintered at 1473 K for different sintering times

It is clearly recorded that the temperature dependences of μ_i become flatter, with poorly pronounced temperature maxima. In addition, the maximum values of $\mu_{i\,max}$ sharply decrease in comparison with the curves in Fig. 3. In this case, the degree of relative decrease in $\mu_{i\,max}$ increases with increasing duration of isothermal sintering. This behavior of the curves indicates an increased defectiveness of the samples sintered at 1473 K and competing processes of healing microstructure defects (pores, phase inclusions, etc.) as well as the formation of new defects due to the decomposition of ferrite. That is, as sintering progresses, the resulting defectiveness decreases (since $\mu_{i\,max}$ increases), but due to deferritization, the rate of its decrease is reduced, despite the higher temperature. At the beginning of isothermal exposure, when the degree of decomposition is low, and the rate of void healing is high, there is a sharp decrease in the total defectiveness and, accordingly, a sharp increase in $\mu_{i\,max}$ to a level characteristic of sintering at 1373 K.

.

Simultaneously with these processes, homogenization of the magnetic phases occurs. It can be seen from Figure 5 that by the beginning of the isothermal stage of sintering, two phases are present in the sample. Then the transition width narrows (τ~ 5 min) and after 15 min only the high-temperature phase remains, which remains until the limiting (τ = 120 min) sintering time. Considering that phase homogenization is associated with diffusion transitions of atoms, the observed increase in the rate of this process with increasing temperature should be recognized as natural. A feature of the crystal chemistry of lithium-containing ferrites is the ordered arrangement of Li^{+} and Fe^{3+} ions in octahedral positions in the (110) direction. Upon slow cooling to a temperature of 750 °C, the structure is ordered. Such a state of ferrite is characterized by a lattice parameter a = 8.329 Å (in disordered ferrite a = 8.332 Å).

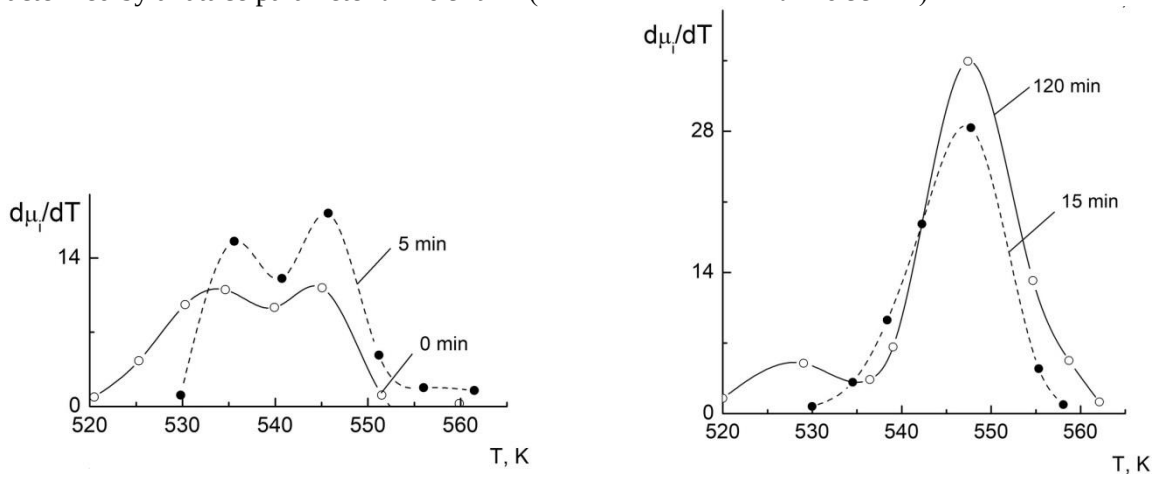

a) b)

Fig.5. Differential temperature dependence of the initial permeability near the Curie temperature for samples sintered at 1373 K for 0, 5 min (a) and 15, 120 min (b) via T mode

It has been established that the magnetic anisotropy constant k of "disordered" ferrite exceeds in absolute value k "ordered" ferrite. The ordering of the ferrite structure also reduces the magnetostriction constant λ_S, but does not affect the saturation magnetization Ms (since the cation distribution does not change in this case). By adjusting the cooling mode of sintered ferrite, one can influence the magnetic permeability of products. In this regard, the relationship between the cooling conditions of the samples and their initial magnetic permeability was studied.

Methodically, the cooling temperature range was divided into two parts: the first part included temperatures from 1370 K (sintering temperature) to 1030 K (cationic freezing temperature); the second is from 1030 K to 530 K (the lower limit of temperature control). Changing the duration of cooling in the first section created different degrees of cationic ordering. At such high temperatures, the samples are quite plastic, and there is no accumulation of thermoelastic stresses (at high cooling rates). And vice versa, when the cooling rate changes only in the second section, the degree of cationic ordering remains constant. The value of thermoelastic stresses can change, since the plasticity of the material at low temperatures is low.

Figure 6a shows the temperature dependences of μ_i at different cooling rates in the high-temperature section. It can be seen that with a decrease in the cooling rate, μ_i monotonically increases, which indicates the importance of the relationship between the cationic ordering and the value of $\mu_{i\,max}$ as well as a slight change in the stoichiometry of the composition at the cooling stage. In contrast to high-temperature cooling, low-temperature variations in the rate of temperature decrease do not lead to noticeable changes in the values of μ_i. As follows from Figure 6b, changes in the cooling rate within 4.1–125 K/min in the temperature range 1030–530 K do not lead to a difference in the temperature dependences of μ_i. Probably, the quenching stresses arising during thermal cooling are insignificant in comparison with the elastic fields created by the coalescence of grains with different crystallographic orientations, as well as various kinds of inclusions in the grain material.

The direct dependences of $\mu_{i\,max}$ on the cooling rate are shown in Figure 7. The specificity of radiation heating of sintered products lies, as is known, in the volumetric nature of heat release. The question arises: do the processes of removal of the technological binder (PVA) and spreading of the liquid phase (Bi_2O_3) over the array of grains of the resulting ferrite have time to complete in a short heating time (~2.5 min). The incompleteness of these processes leads to a deterioration in the quality of products.

The temperature dependences of μ_i were studied both on the rate of heating of press samples during their sintering and on the isothermal exposures during their heating. For this, the isothermal sintering was carried out at 1373 K for 60 min.

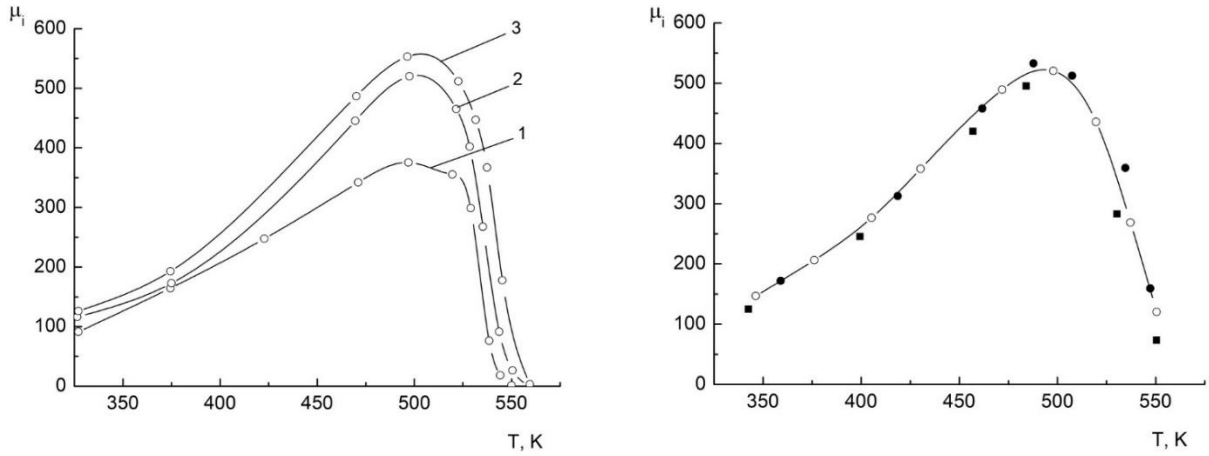

a) b)

Fig.6. Temperature dependence of the initial permeability of ferrite with Bi_2O_3 sintered *via* RT mode at 1373 K for 2 h: (a) – high-temperature cooling during sintering at rates of 68 K/min (curve 1); 5.7 K/min (curve 2); 2.8 K/min (curve 3); (b) –low-temperature cooling at a rate of 4.1 K/min (•); 2.5 K/min (o); 125 K/min (■)

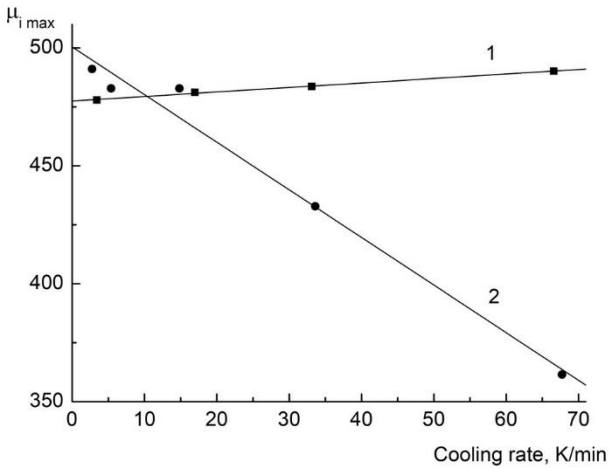

Fig.7. Dependence of $\mu_{i\ max}$ on the cooling rate: high-temperature cooling section (curve 1); low-temperature cooling section (curve 2)

The cooling rate was constant and amounted to 25 K/min. The results of $\mu_{i\ max}$ measurements (Fig. 8) indicate that a change in the rate of radiative heating by two orders of magnitude of pressed samples does not cause changes in the value of $\mu_{i\ max}$.

.

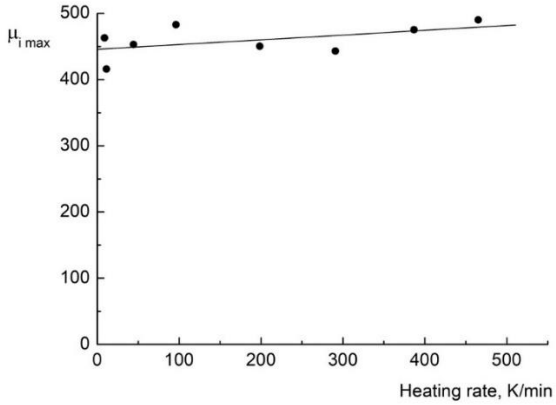

Fig.8. Dependence of $\mu_{i\,max}$ on the radiative heating rate of pressed samples up to a sintering temperature of 1373 K

In addition, isothermal exposures were carried out at characteristic points at the PVA removal temperature (673 K) and at the melting point of the Bi_2O_3 additive (1093 K). The exposure time was varied within 10–60 min, the sample heating rate between the characteristic temperatures was 450 K/min. The results showed that the presence of isothermal exposures does not affect the nature of the temperature dependence of μ_i and the value of $\mu_{i\,max}$.

Conclusion

The scientific significance of the results is determined by the data on the initial magnetic permeability, as well as the relationship of this characteristic with phase changes in ferrite sintered under conditions of electron beam heating. It was shown that the presence of a low-melting additive Bi_2O_3 leads to a more defect-free state of the ferrite. This effect is enhanced by the action of radiation at the early stages of ferrite sintering by an electron beam. It was established for the first time that a change in the rate of radiative heating by two orders of magnitude and isothermal holding at the temperature of removal of polyvinyl alcohol (673 K) and melting of Bi_2O_3 (1093 K) do not affect the phase composition of the LiTiZnMn ferrite. Low-temperature variations in the cooling rate after sintering of the compacts do not lead to noticeable changes in the initial permeability. A decrease in the cooling rate in the high-temperature sintering region is accompanied by a monotonic increase in the initial permeability.

Acknowledgments

The research was supported by The Ministry of Science Higher Education of the Russian Federation in part of the Science program (Project FSWW–2023–0011).

REFERENCES

1 Lysenko E.N., Nikolaev E, Vlasov V.A., Surzhikov A.P. Microstructure and reactivity of Fe2O3-Li2CO3-ZnO ferrite system ball-milled in a planetary mill. *Thermochimica Acta*, 2018, Vol. 664, pp. 100 – 107.

2 Minin V.M. Effect of sintering conditions on the microstructure and electromagnetic properties of Li-Mg-Mn ferrite memory elements. *Soviet Powder Metallurgy and Metal Ceramics*. 1982, Vol. 21, pp. 698 – 701.

3 Zahir R., Chowdhury F.-U.-Z., Uddin M.M., et al. Structural, magnetic and electrical characterization of Cd substituted Mg ferrites synthesized by double sintering technique. *J. Magn. Magn. Mater*. 2016, Vol. 410, pp. 55 – 62.

4 Manjura Hoque S., Abdul Hakim M., Mamun Al, et al. Study of the bulk magnetic and electrical properties of $MgFe_2O_4$ synthesized by chemical method. *Materials Sciences and Applications*. 2011, Vol. 2, pp. 1564 – 1569.

5 Surzhikov A.P., Pritulov A.M., Lysenko E.N., et al. Calorimetric investigation of radiation-thermal synthesized lithium pentaferrite. *Journal of Thermal Analysis and Calorimetry*. 2010, Vol. 101, No. 1, pp. 11 – 13.

6 Zhuravlev V.A., Naiden E.P., Minin R.V., Itin V.I., Suslyaev V.I., Korovin E.Yu. Radiation-thermal synthesis of W-type hexaferrites. *IOP Conference Series Materials Science and Engineering*. 2015, Vol. 81, 012003.

7 Naiden, E.P., Zhuravlev, V.A., Minin, R.V., Suslyaev, V.I., Itin, V.I., Korovin, E. Yu. Structural and magnetic properties of SHS-produced multiphase W-type hexaferrites: influence of radiation-thermal treatment. *International Journal of Self-Propagating High-Temperature Synthesis*, 2015, Vol. 24, pp. 148 – 151.

8 Zhuravlev V.A., et al. Computer simulation of processes of radiation-thermal heating. *IOP Conference Series: Materials Science and Engineering*, 2015, Vol. 81, 012054. doi:10.1088/1757-899X/81/1/012054

9 Ancharova U.V., Mikhailenko M.A., Tolochko B.P., et al. Synthesis and Staging of the Phase Formation for Strontium Ferrites in Thermal and Radiation Thermal Reactions. *IOP Conference Series Materials Science and Engineering*, 2015, Vol. 81, 012122. doi:10.1088/1757-899X/81/1/011001

10 Ning K., Lu J., Xie P., et al. Study on surface modification of silicone rubber for composite insulator by electron beam irradiation. *Nuclear Instruments and Methods in Physics Research Section B: Beam Interactions with Materials and Atoms*, 2021, Vol. 499, pp. 7 – 16. doi:10.1016/j.nimb.2021.04.019

11 Chettri P., Deka U., Rao A., Nagaraja K.K., et al, Dwivedi J. Effect of high energy electron beam irradiation on the structural properties, electrical resistivity and thermopower of $La_{0.5}Sr_{0.5}MnO3$ manganites. *Physica B: Condensed Matter*, 2020, Vol. 585, 412119. doi:10.1016/j.physb.2020.412119

12 Oane M., Toader D., Iacob N., Ticos C.M. Thermal phenomena induced in a small tungsten sample during irradiation with a few MeV electron beam: Experiment versus simulations. *Nuclear Instruments and Methods in Physics Research Section B: Beam Interactions with Materials and Atoms*, 2014, Vol. 337, pp. 17 – 20.

13 Salimov R.A., Cherepkov V.G., Kuksanov N.K., Kuznetzov, S.A. The use of electron accelerators for radiation disinfestation of grain, *Radiation Physics and Chemistry*, 2000, Vol. 57, pp. 625 – 627.

14 Salimov R.A., Cherepkov V.G., Golubenko J.I., et al. D.C. high power electron accelerators of ELV-series: status, development, applications. *J. Radiation Phys. Chem.* 2000, Vol. 57, pp. 661 – 665.

15 Cleland M.R., Parks L.A. Medium and high-energy electron beam radiation processing equipment for commercial applications. *Nucl. Instr. Meth. B.* 2003, Vol. 208, pp. 74 – 89.

16 Mehnert R. Review of industrial applications of electron accelerators. *Nucl. Instr. Meth. B* 1996, Vol. 113, pp.81–87.

17 Neronov V.A., Voronin A.P., Tatarintseva M.I., Melekhova T.E., Auslender V.L. Sintering under a high-power electron beam. *J. Less-Common Metals*. 1986, Vol. 117, pp. 391 – 394.

18 Kostishyn V., et al. Obtaining anisotropic hexaferrites for the base layers of microstrip SHF devices by the radiation-thermal sintering. *Eastern-European Journal of Enterprise Technologies*, 2016, Vol. 5, pp. 32 – 39.

19 Kostishin V.G., Andreev V.G., Korovushkin V.V., et al. Preparation of 2000NN ferrite ceramics by a complete and a short radiation-enhanced thermal sintering process. *Inorganic Materials*, 2014, Vol, 50, pp. 1317 – 1322.

20 Malyshev A.V., Lysenko E.N., Vlasov V.A., Nikolaeva S.A. Electromagnetic properties of $Li_{0.4}Fe_{2.4}Zn_{0.2}O_4$ ferrite sintered by continuous electron beam heating, *Ceramics International*, 2016, Vol. 42, pp. 16180 – 16183.

21 Neronov V.A., Voronin A.P., Tatarintseva M.I., Melekhova T.E., Auslender V.L. Sintering under a high-power electron beam. *Journal of the Less-Common Metals*, 1986. Vol. 117, pp. 391 – 394.

22 Solodkyi I., Bogomol I., Loboda P. High-speed electron beam sintering of WC-8Co under controlled temperature conditions, *International Journal of Refractory Metals and Hard Materials*, 2022, Vol. 102, 105730.

23 Auslender V.L. ILU-type electron accelerator for industrial technologies. *Nuclear Instruments and Methods in Physics Research Section B: Beam Interactions with Materials and Atoms*, 1994, Vol. 89, pp. 46 – 48.

24 Auslender V.L., Bryazgin A.A., Faktorovich B.L., Gorbunov V.A., Kokin E.N., Korobeinikov M.V., Voronin L.A. Accelerators for E-beam and X-ray processing, *Radiation Physics and Chemistry*, 2002, Vol. 63, pp. 613 – 615.

25 Tyutnev A.P., Saenko V.S., Vannikov A.V, Oskin V.E. Radiation induced dielectric effect in polymers, *Physica Status Solidi (a)*, 1984, Vol. 86, pp. 363 – 374.

26 Boev S.G. Kinetics of charge formation in electron-irradiated dielectrics, *Soviet Surface Engineering and Applied Electrochemistry*, 1987, Vol. 2, pp. 69 – 72.

27 Lysenko E.N., Malyshev A.V., Vlasov V.A., et al. Microstructure and thermal analysis of lithium ferrite pre-milled in a high-energy ball mill. *Journal of Thermal Analysis and Calorimetry*, 2018, Vol. 134, No. 1, pp. 127 – 133.

28 Surzhikov A.P., Lysenko E.N., et al. Thermogravimetric investigation of the effect of annealing conditions on the soft ferrite phase homogeneity. *Journal of Thermal Analysis and Calorimetry*. 2011, Vol. 104, No. 2, pp. 613 – 617.

29 Stary O., Malyshev A.V., Lysenko E.N., Petrova A. Formation of magnetic properties of ferrites during radiation-thermal sintering. *Eurasian phys. tech. j.* 2020, Vol. 17, No. 2, pp. 6 – 10.

30 Surzhikov A.P., Frangulyan, T.S., Ghyngazov, S.A., Vasil'ev, I.P., Chernyavskii, A.V. Sintering of zirconia ceramics by intense high-energy electron beam. *Ceramics Int.* 2016, Vol. 42, No. 12, pp. 13888 – 13892.

31 Nikolaev E.V., Astafyev A.L., Nikolaeva S.A., Lysenko E.N., Zeinidenov A.K. Investigation of electrical properties homogeneity of Li-Ti-Zn ferrite ceramics. *Eurasian phys. tech. j.* 2020, Vol. 17, No. 1, pp. 5 – 12.

32 Surzhikov A.P., Malyshev A.V., Lysenko E.N., Stary O. Temperature dependences of the initial permeability of lithium-titanium ferrites produced by solid-state sintering in thermal and radiation-thermal modes. *Eurasian phys. tech. j.* 2022, Vol. 19, No, 1, pp. 5 – 9.

33 Smith J., Wijn H.P.J. Ferrites: *Physical properties of ferromagnetic oxides in relation to their technical application.* 1959, Eindhoven, Phillips Technical Library, 233p.

34 Grishaev V.V., Lebed' B.M., Marchik I.I. Radiation-stimulated sintering of powder materials. *Electronic equipment. Ser. Materials.* 1983, Issue 5, pp. 13 – 17. [in Russian]

35 Letyuk L.M., et al. Special features of the formation of the microstructure of ferrites sintered in the presence of a liquid phase. *Izv.Vysshikh Uchebnykh Zavedenij - Chernaya Metallurgiya*. 1979, Vol. 11, pp. 124 – 127. [in Russian]

Article accepted for publication 20.03.2023

.